Supporting Information for

Lanthanide Metal-Organic Frameworks for Catalytic Oxidation of Olefins

Y B. N. Tran,[ab] and Phuong T. K. Nguyen,[*ab]

[a]Future Materials & Devices Laboratory, Institute of Fundamental and Applied Sciences, Duy Tan University, Ho Chi Minh City 700000, Viet Nam

[b]Faculty of Natural Sciences, Duy Tan University, Da Nang, 550000, Viet Nam.

*To whom correspondence should be addressed: Email, nguyentkieuphuong1@duytan.edu.vn.

Table of Contents

Section S1: Materials and Analytical Techniques

Chemical used in this work.

Lanthanum (III) nitrate hydrate ($La(NO_3)_3 \cdot xH_2O$, 99.9%), 1,4,5,8-naphthalenetetracarboxylic dianhydride (NTCDA), glacial acetic acid (≥99.85%), anhydrous *tert*-butyl hydroperoxide (TBHP, 5.0 – 6.0 M in decane), *tert*-butyl hydroperoxide solution (70% in H_2O), cerium (IV) oxide (CeO_2, ≥99.0%), trimesic acid (H_3BTC, 95%), and 2,2,6,6-tetramethylpiperidine 1-oxyl (TEMPO, 98%), were obtained from Sigma-Aldrich. 5-aminoisophthalic acid (≥98%), *N,N*-dimethylformamide (DMF, 99.8%), anhydrous ethanol (EtOH, 99.5%), styrene (99.5%), cyclohexene (99%), and chlorobenzene (99,5%) were purchased from Acros Organics. Cerium (III) nitrate hexahydrate ($Ce(NO_3)_3 \cdot 6H_2O$, ≥98.5%), lanthanum(III) oxide (La_2O_3, ≥99.5%), sodium periodate ($NaIO_4$, ≥99.0%), hydrogen peroxide (H_2O_2, 30%), *N,N*-dimethylacetamide (DMA, ≥99.0%), and ethyl acetate (EtOAc, ≥99.5%) were obtained from Merck Chemical Co. Deionized water (ultrapure, 17.8 MΩ·cm resistivity, obtained from a Barnstead Easypure II system). Deuterated solvents, $CDCl_3$ and DMSO-d_6, were purchased from Cambridge Isotope Laboratories (Andover, MA) and used without further purification. All chemicals were used without further purification unless otherwise noted.

MOF-177 (Basolite Z377), ZIF-8 (Basolite Z1200), MIL-53(Al) (Basolite A100), and HKUST-1 (Basolite C300) were purchased from Sigma-Aldrich. To yield guest-free material, MOF-177, and ZIF-8 were activated under vacuum (10^{-3} Torr) and heated at 120°C for 24 h. MIL-53(Al) was immersed in anhydrous methanol (5 mL) for 1 day before activated under vacuum at ambient temperature for 12 h, followed by heating at 100 °C under vacuum for an additional 24 h.

Synthesis of Ce-MOF-76, $[Ce(BTC)] \cdot 2H_2O \cdot DMF)$:[S1] Ce-MOF-76 was synthesized, with slight modifications, according to a previously reported procedure.[S1] A 0.124 M stock solution of cerium(III) nitrate hexahydrate in H_2O (1 mL) was added to Pyrex tube (o.d. × i.d. = 10 mm × 12 mm), which was preloaded with benzene-1,3,5-tricarboxylic acid H_3BTC (13.1 mg, 0.062 mmol). This was followed by the addition of DMF (4 mL) and deionized water (2 mL). The tube was then sealed, sonicated for 30 min, and heated at 140 °C to get white powder. The powder was then thoroughly washed with DMF (3 ✕ 10 mL per day, for a total 3 days). To yield guest-free material, the DMF-wash sample MOF-76-Ce was subsequently immersed in EtOH (4 ✕ 10 mL per day over a period of 3 days). The EtOH-exchanged sample was activated under vacuum at room

temperature for 24 h, followed by heating at 80 °C for an additional 24 h. Calcd for $Ce(C_9H_3O_6)\cdot 2H_2O\cdot(C_3H_7NO)$: C, 31.58; H, 3.09; N, 3.07%. Found: C, 31.43; H, 3.17; N, 3.11%.

Analytical techniques.

Powder X-ray diffraction (PXRD) data were collected using a Bruker D8 Advance employing Ni-filtered Cu Kα (λ = 1.54178 Å). The system was also outfitted with an anti-scattering shield that prevents incident diffuse radiation from hitting the detector. Samples were placed on zero background sample holders by dropping powders from a spatula and then leveling the sample with a spatula. The 2θ range was 3-50° with a step size of 0.02° and a fixed counting time of 1 s per step. Fourier transform infrared (FT-IR) spectra were measured using KBr pellets on a Bruker Vertex 70 system, and the output signals are described as follows: vs, very strong; s, strong; m, medium; sh, shoulder; w, weak; vw, very weak; br, broad. Electrospray-ionization mass spectrometry (ESI-MS) was conducted in negative ionization mode on an Agilent 1200 Series high-performance liquid chromatography coupled to a Bruker micrOTOF-QII mass spectrometer detector. Field-emission Scanning Electron Microscope (FE-SEM) was performed on an ultralow voltage imaging with Hitachi's S-4800 FE-SEM operating at an accelerating voltage of 1 kV. The Ce-MOF-589 sample was by dispersed onto a sticky carbon surface attached to a flat aluminum sample holder.

Gas chromatography (GC) analyses were carried out using an Agilent GC System 123-0132 equipped with a flame ionization detector (FID) and a capillary DB-1ms column (30 m × 320 μm × 0.25 μm) with the use of chlorobenzene as an internal standard. The temperature program for GC-FID analysis was set as follows: the temperature was held at 50 °C for 2 min, then raised to 250 °C at 25 °C /min and held for 4 min, using nitrogen as a carrier gas, split flow 188.82 ml/min, pressure 8.4845 psi. Inlet and detector temperatures were 250 °C and 300 °C, respectively. GC-MS analyses were performed on an Agilent GC System 19091S-433: 93.92873 equipped with a mass spectroscopy detector (Agilent GCMSD - 5977A) using a capillary HP-5MS 5% Phenyl Methyl Silox column (30 m × 250 μm × 0.25 μm) using helium as a carrier gas, the temperature of MS source (230 °C - 250 °C) and MS Quad (150 °C - 200 °C). The temperature program for GC-MS analysis of styrene oxidation was set as follows: initial temperature was held at 50 °C for 1 min, then raised to 300 °C at 20 °C /min and held for 10 min, split ratio 100: 1, split flow 77.673 mL/min, pressure 5 psi. The temperature program for GC-MS analysis of cyclohexene oxidation

was set as follows: initial temperature at 50 °C for 1 min, then raised to 300 °C at 20 °C /min and held for 10 min, split ratio 25 : 1, split flow 13.953 mL/min, pressure 2 psi.

Section S2: Optical Images, Powder X-Ray Diffraction, and Structural Refinement of Ln-MOF-589

Optical Images

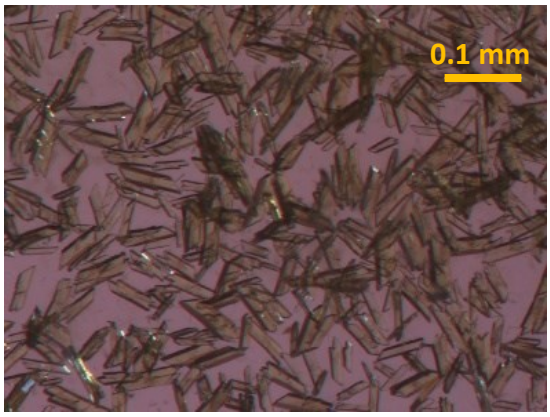

Figure S1. Optical microscope image of La-MOF-589 showing homogenous crystal morphology.

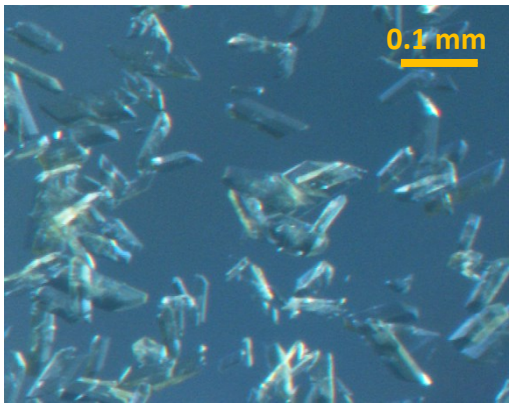

Figure S2. Optical microscope image of Ce-MOF-589 showing homogenous crystal morphology.

Powder X-Ray Diffraction (PXRD)

Experimental PXRD patterns were recorded using a Bruker D8 Advance diffractometer with Ni-filtered Cu Kα radiation (λ = 1.5418 Å), a Lynxeye detector with Ni-filtered low β (1.56%) and slit size (12.75 mm). The Bragg-Brentano diffraction geometry consists of mounted optics: Göbel mirror, fixed divergence slit (0.6 mm), receiving slit (3 mm), primary and secondary beam Soller slits (2.5°). Void space was determined by using Calc Void function in PLATON package.

The initial crystal model of the La-MOF-589 structure was constructed by replacing Ce^{3+} of Ce-MOF-589 with La^{3+}, and the triclinic space group $P\bar{1}$ was retained. Full profile pattern matching Pawley refinements were evaluated in 2θ range from 4 to 50° using *Reflex* module. A Pseudo-Voigt was employed to define the peak profile. The unit cell parameters *a*, *b*, *c*, FWHM parameters U, V, W, profile parameters NA, NB, zero point, shift#1, and shift#2 were refined. The background coefficients were refined with 10th order polynomial. The refined unit cell parameters for La-MOF-589 were compared with the initial crystal model and the fractional atomic coordinates were provided in Tables S1.

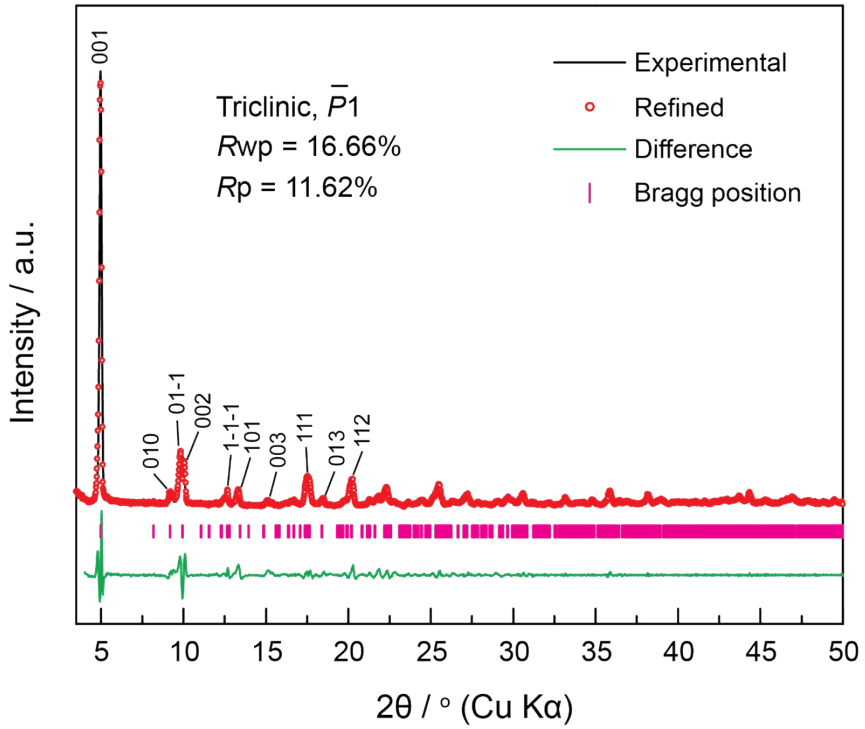

Figure S3. The Pawley refinement of La-MOF-589. Shown are the experimental (black), refined (red), and difference (green) patterns. The Bragg positions are marked as pink bars.

Table S1. Unit cell parameters and fractional atomic coordinates for the refined crystal model La-MOF-589.

Empirical formula, Space group	$C_{30}H_{17}LaN_2O_{15}$, $P\bar{1}$
Refined unit cell	*a* = 8.2030 Å, *b* = 11.0561 Å, *c* = 17.4692 Å, α = 93.2554°, β =

		95.5703°, γ = 107.6232°.			
Pawley refinement		R_{wp} = 16.66%, R_{wp} (w/o background) = 8.32%, R_p = 11.62%			
Atom label	Atom type	*x*	*y*	*z*	Site Occupancy
La1	La	0.10861	0.1504	-0.11079	1
C1	C	0.07776	0.16183	0.09511	1
C2	C	-0.09323	0.55812	0.09279	1
C3	C	-0.00686	0.47544	0.13428	1
C4	C	-0.00348	0.36171	0.09737	1
C5	C	0.06864	0.28147	0.13683	1
C6	C	0.13063	0.31137	0.21428	1
C7	C	0.13104	0.42632	0.24985	1
C8	C	0.0666	0.51035	0.21058	1
C9	C	0.08965	0.39416	0.38396	1
C10	C	0.1504	0.43409	0.4669	1
C11	C	0.06004	0.36814	0.52225	1
C12	C	0.11167	0.41018	0.60089	1
C13	C	0.24773	0.5184	0.62288	1
C14	C	0.29578	0.56491	0.70565	1
C15	C	0.52231	0.75417	0.67096	1
C16	C	0.48153	0.69906	0.58873	1
C17	C	0.57805	0.76053	0.53388	1
C18	C	0.53583	0.71276	0.45571	1
C19	C	0.3965	0.606	0.43323	1
C20	C	0.35316	0.55555	0.35086	1
C21	C	0.29589	0.54268	0.48826	1
C22	C	0.34189	0.58775	0.56723	1
C23	C	0.4382	0.74236	0.80157	1
C24	C	0.37795	0.84456	0.81572	1
C25	C	0.39066	0.8965	0.89143	1
C26	C	0.46371	0.84489	0.95186	1
C27	C	0.52303	0.74218	0.93636	1

C28	C	0.50838	0.68953	0.86046	1
C29	C	0.31751	1.00331	0.90734	1
C30	C	0.60765	0.68793	0.99957	1
O1	O	0.08637	0.16117	0.02421	1
O2	O	0.07582	0.07024	0.13473	1
O3	O	-0.19825	0.50302	0.03342	1
O4	O	-0.06188	0.67181	0.11738	1
O5	O	0.44721	0.59223	0.30228	1
O6	O	-0.04395	0.31104	0.36191	1
O7	O	0.63788	0.85071	0.69242	1
O8	O	0.23165	0.50383	0.75656	1
O9	O	0.29097	1.06773	0.852	1
O10	O	0.2799	1.02533	0.97334	1
O11	O	0.63327	0.73928	1.0677	1
O12	O	0.65335	0.59287	0.97903	1
O1W	O	-0.20286	0.13407	-0.08555	1
O2W	O	-0.0834	0.09383	-0.24268	1
O3W	O	0.267	0.27467	-0.21599	1
N1	N	0.19374	0.45921	0.33148	1
N2	N	0.4173	0.68591	0.72304	1
H1WA	H	-0.23525	0.08028	-0.05232	1
H1WB	H	-0.27102	0.1094	-0.12766	1
H2WA	H	-0.18244	0.04058	-0.23733	1
H2WB	H	-0.03521	0.05928	-0.27573	1
H3	H	-0.23096	0.4259	0.03674	1
H3WA	H	0.37596	0.28178	-0.20881	1
H3WB	H	0.25625	0.35036	-0.21472	1
H4	H	-0.04975	0.33939	0.04592	1
H6	H	0.17145	0.25498	0.24201	1
H8	H	0.07235	0.58889	0.23479	1
H11	H	-0.0345	0.29619	0.50756	1

H12	H	0.05302	0.36432	0.63823	1
H17	H	0.67104	0.83352	0.54858	1
H18	H	0.60244	0.75357	0.41897	1
H24	H	0.32946	0.87824	0.77513	1
H26	H	0.47249	0.87934	1.00247	1
H28	H	0.54574	0.61955	0.84991	1

Section S3: Characterizations of Ln-MOF-589 and Other MOFs.

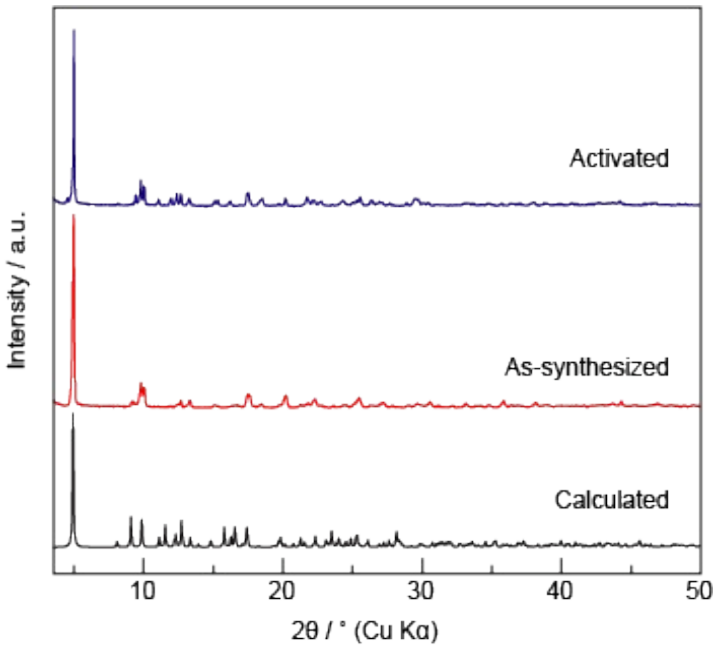

Figure S4. Comparison of the calculated (black) PXRD pattern from the single crystal data with the experimental as-synthesized (red) and activated (blue) PXRD patterns of La-MOF-589.

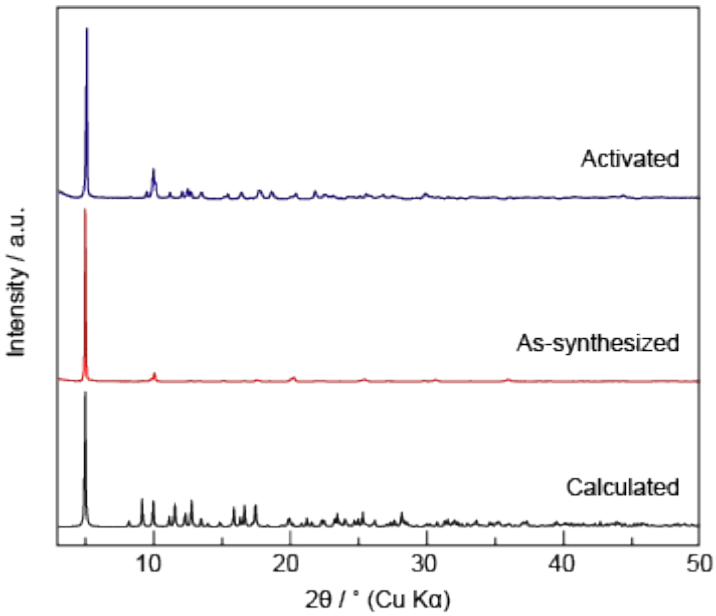

Figure S5. Comparison of the calculated (black) PXRD pattern from the single crystal data with the experimental as-synthesized (red) and activated (blue) PXRD patterns of Ce-MOF-589.

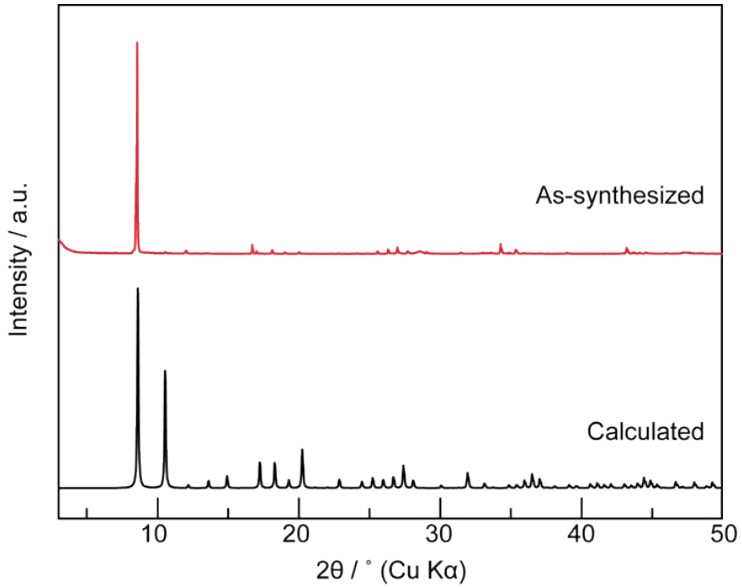

Figure S6. Comparison of the simulated (black) PXRD pattern from the single crystal data with the experimental as-synthesized (red) PXRD patter of Ce-MOF-76.

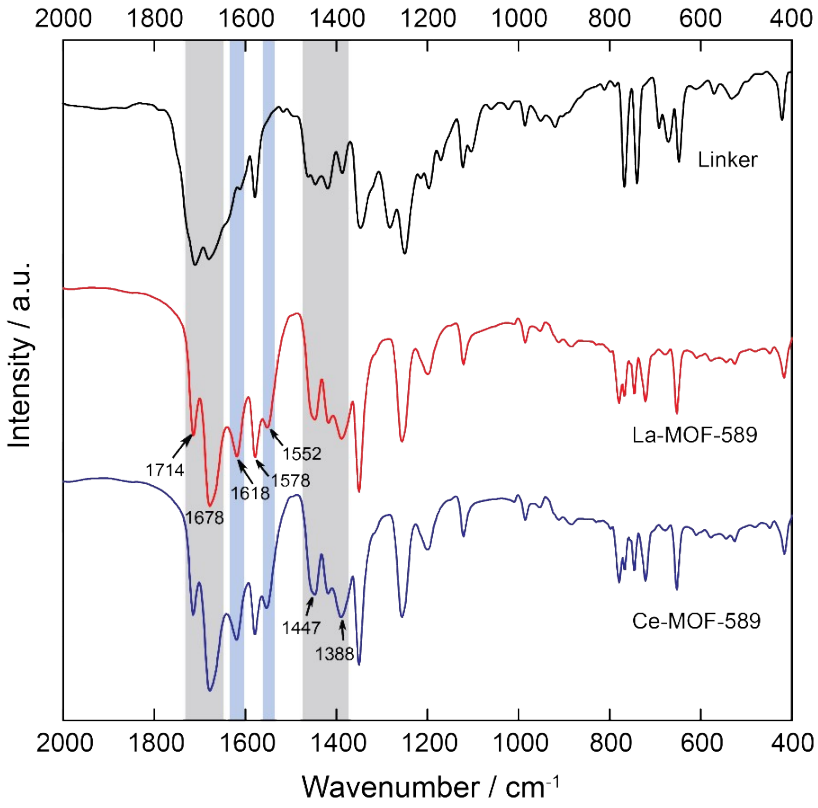

Figure S7. FT-IR spectra of H_4BIPA-TC linker (black), La-MOF-589 (red), and Ce-MOF-589 (blue).

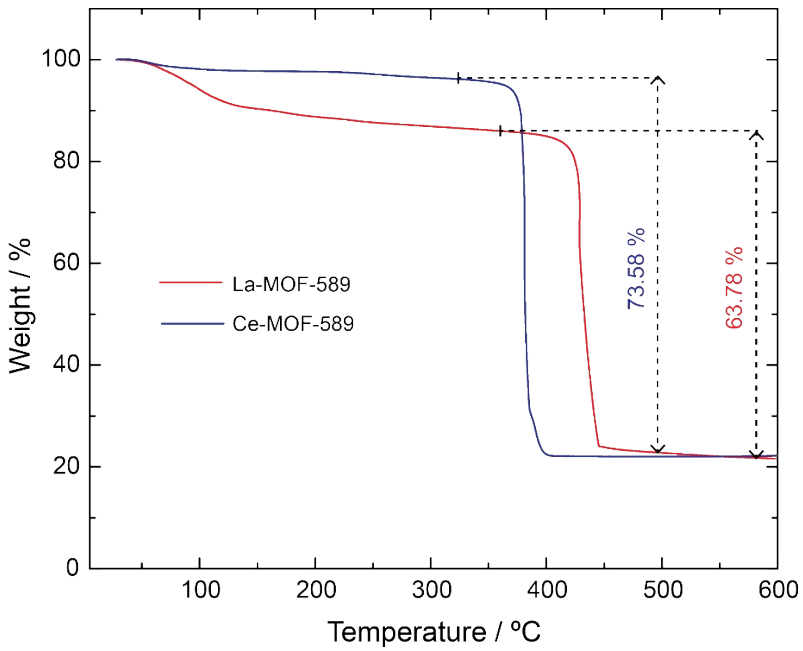

Figure S8. TGA traces of activated La-MOF-589 and Ce-MOF-589 at a heating rate of 5 °C min $^{-1}$ under air flow.

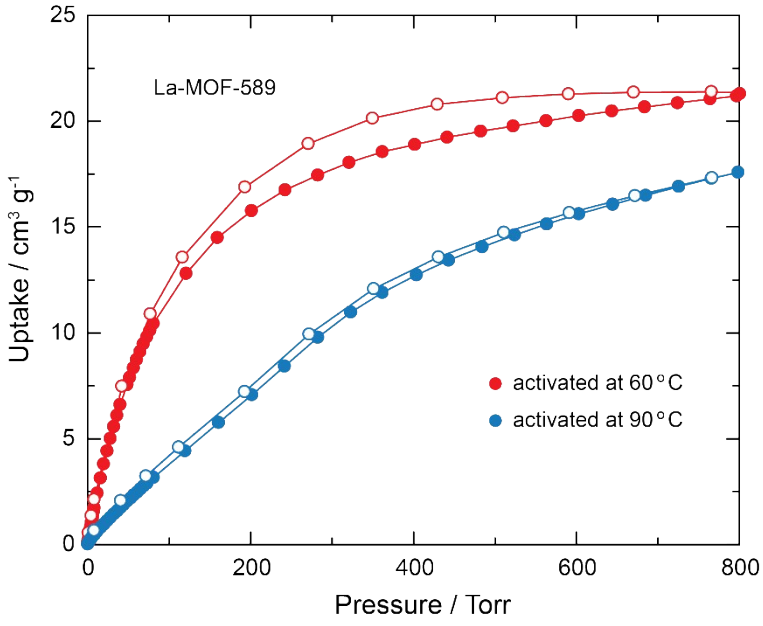

Figure S9. CO_2 isotherms at 273 K of La-MOF-589 activated at 60 °C (red) and 90 °C (blue). Filled and open symbols represent adsorption and desorption branches, respectively. The connecting curves are guides for the eye.

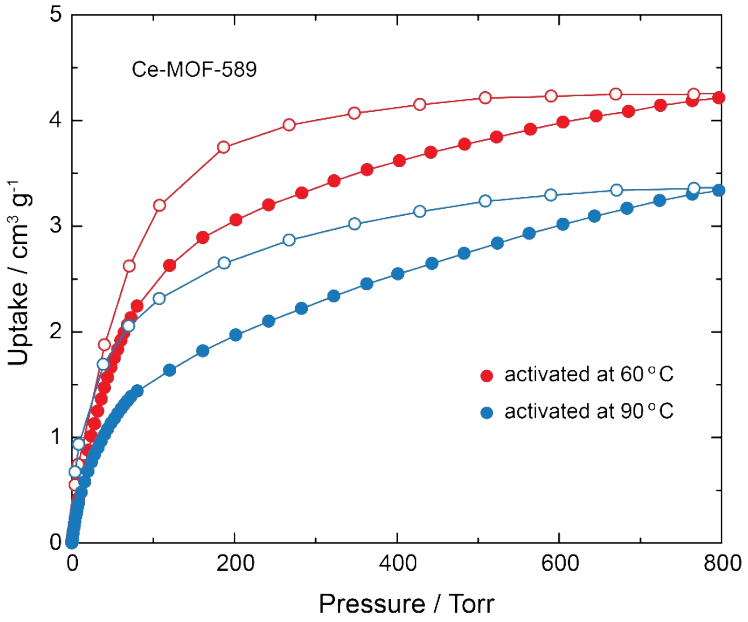

Figure S10. CO_2 isotherms at 273 K of Ce-MOF-589 activated at 60 °C (red) and 90 °C (blue). Filled and open symbols represent adsorption and desorption branches, respectively. The connecting curves are guides for the eye.

Section S4: General Procedure and Studies for the Oxidation of Olefin

The products identification was achieved in GC-FID from the retention time of the pure compounds. Retention time of each product is determined as: styrene, T_R = 3.921 min; benzaldehyde, T_R = 4.445 min; phenylacetaldehyde, T_R = 5.055 min; styrene oxide, T_R = 5.263 min. The conversion of olefin was calculated from moles of olefin consumed against the initial moles of olefin used. The selectivity of epoxide product was determined from moles of the epoxide formed against the moles of olefin consumed, respectively. The yield was calculated from moles of the epoxide formed against the initial moles of olefin used.

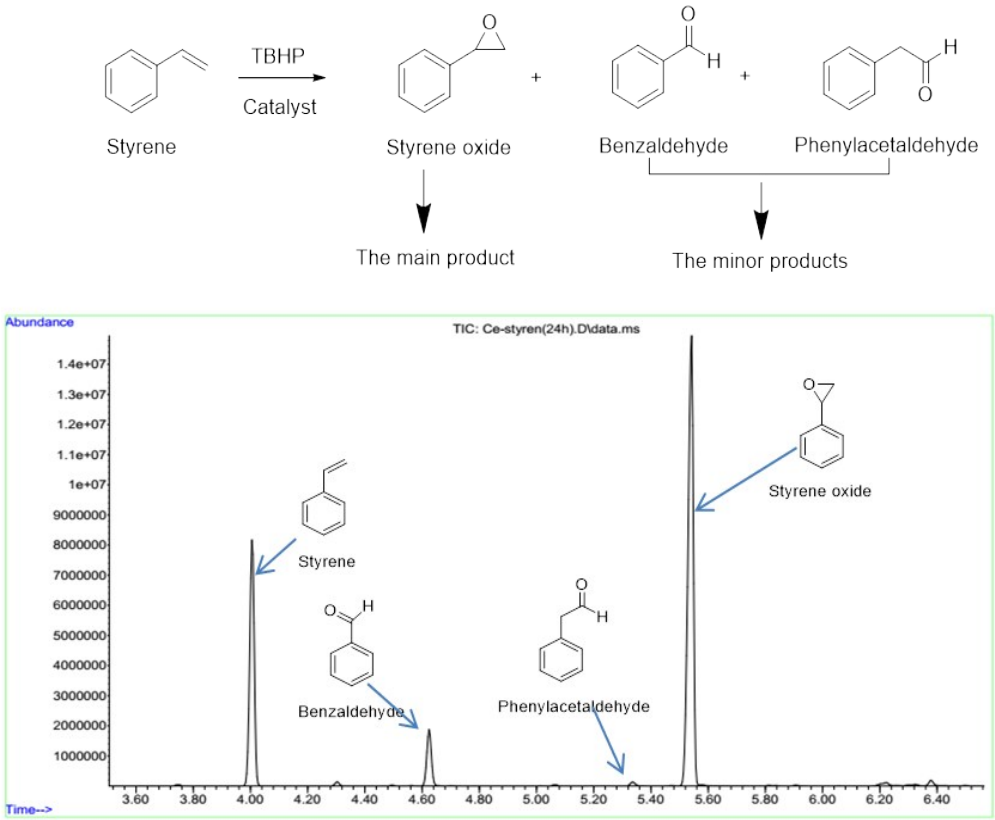

Figure S11. GC chart of a reaction mixture of the styrene oxidation catalyzed by Ce-MOF-589.

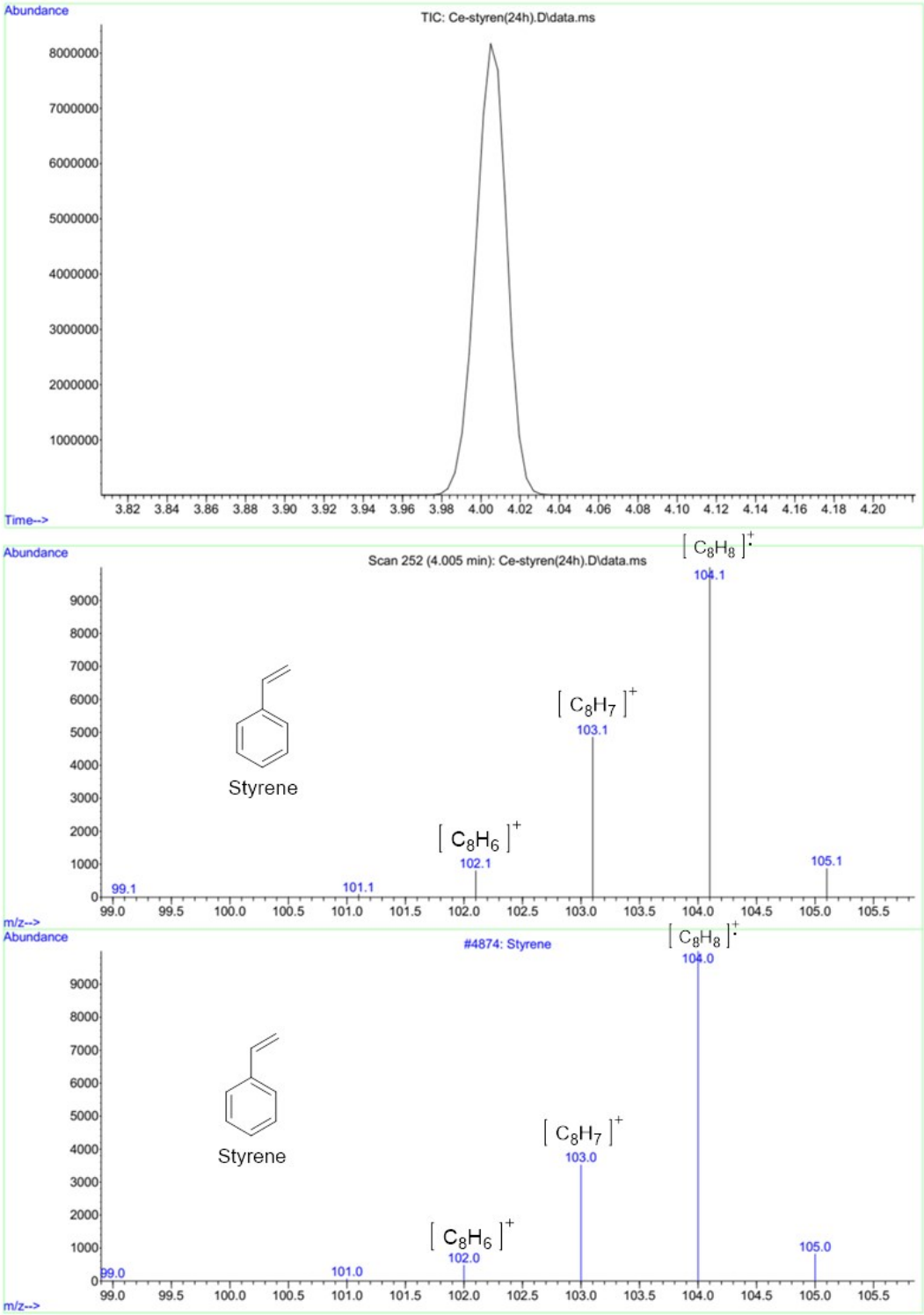

Figure S12. Mass spectrum of styrene.

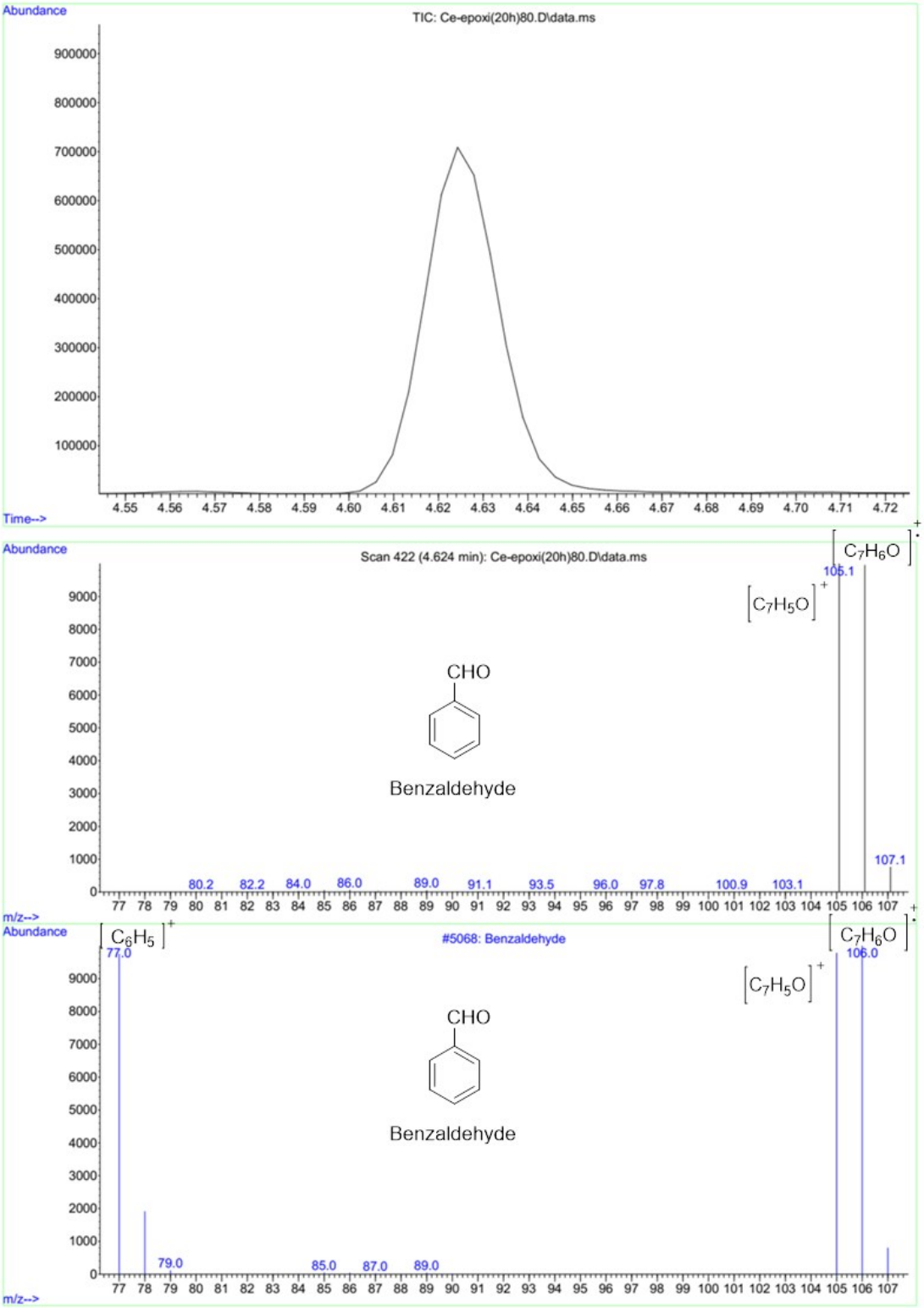

Figure S13. Mass spectrum of benzaldehyde.

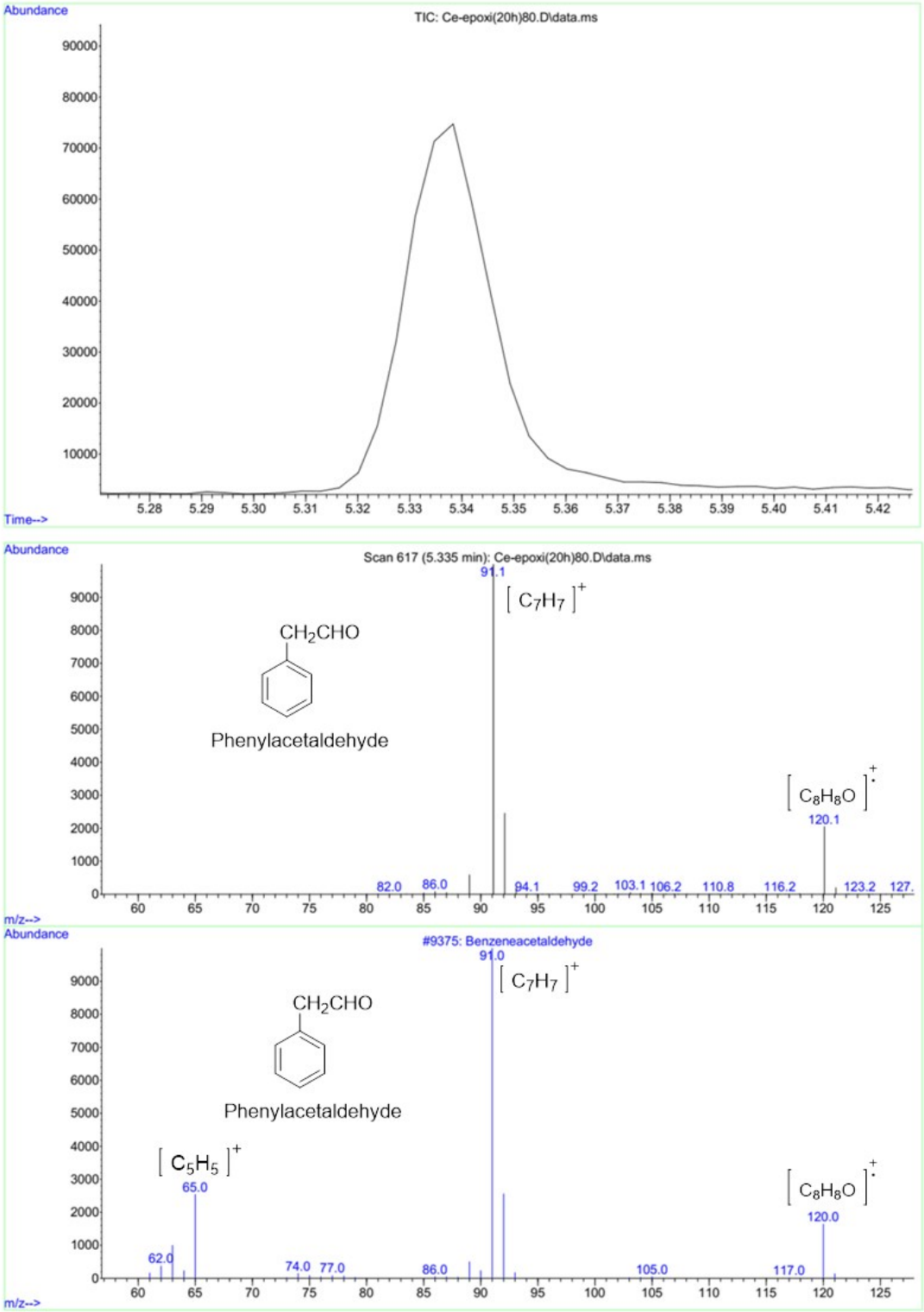

Figure S14. Mass spectrum of phenylacetaldehyde.

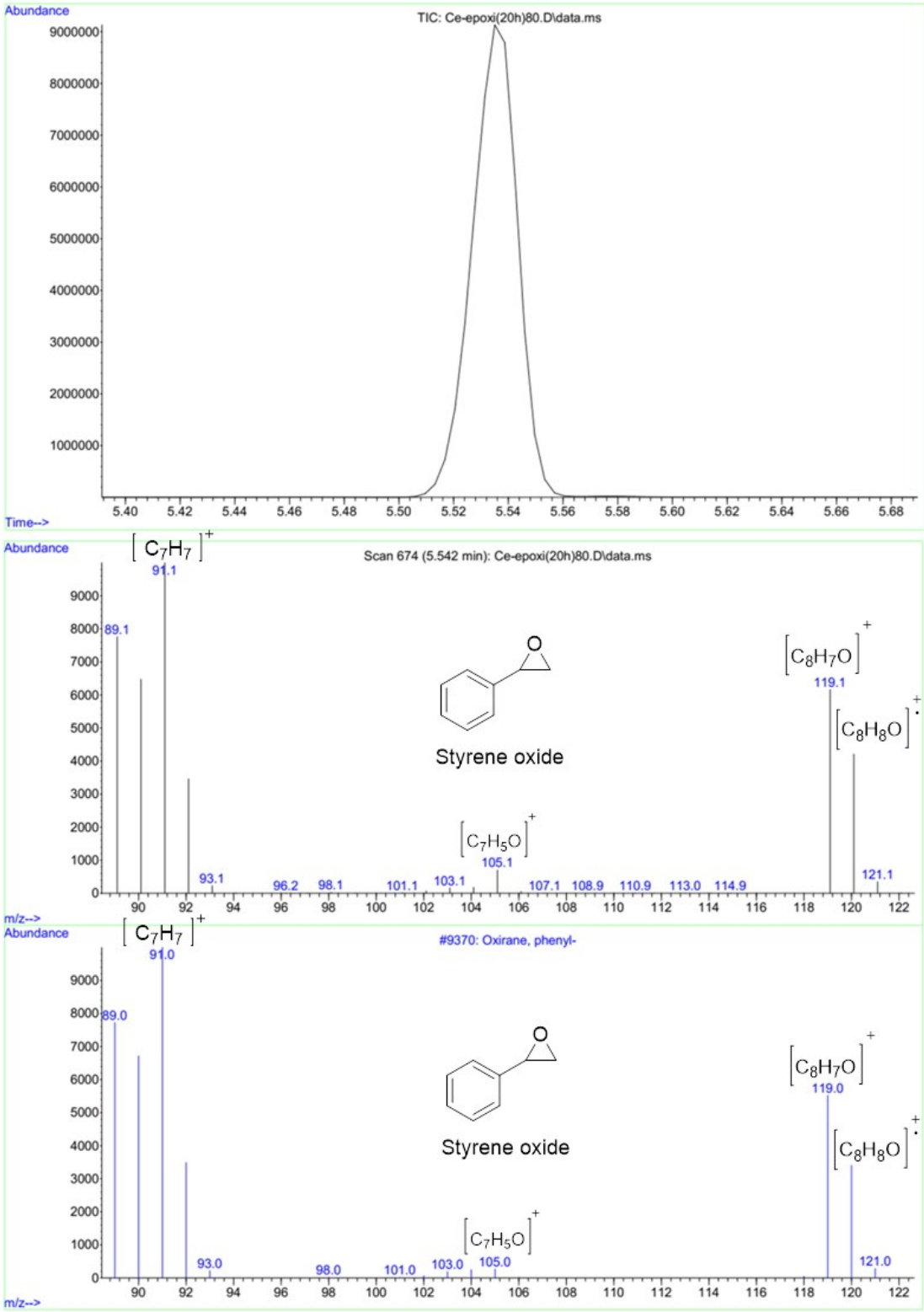

Figure S15. Mass spectrum of styrene oxide.

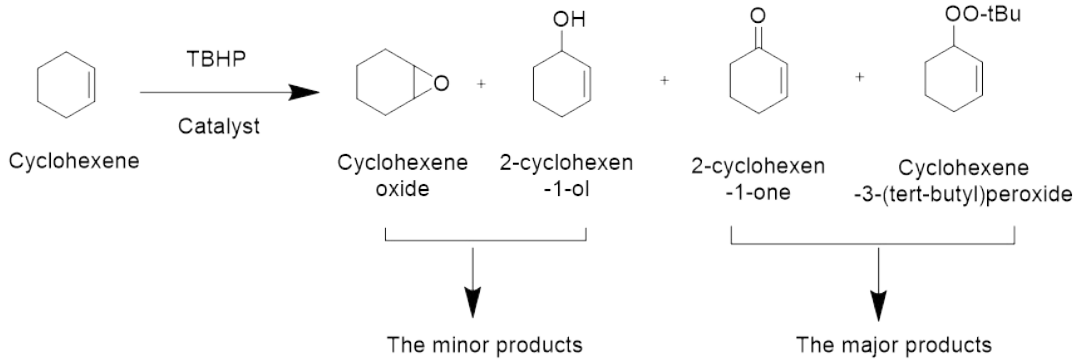

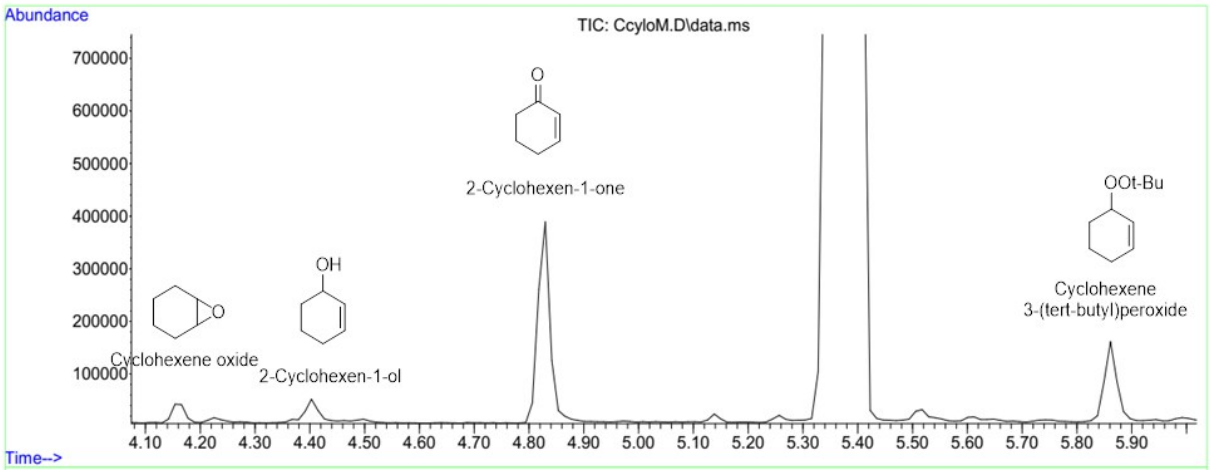

Figure S16. GC chart of a reaction mixture of the cyclohexene oxidation catalyzed by Ce-MOF-589.

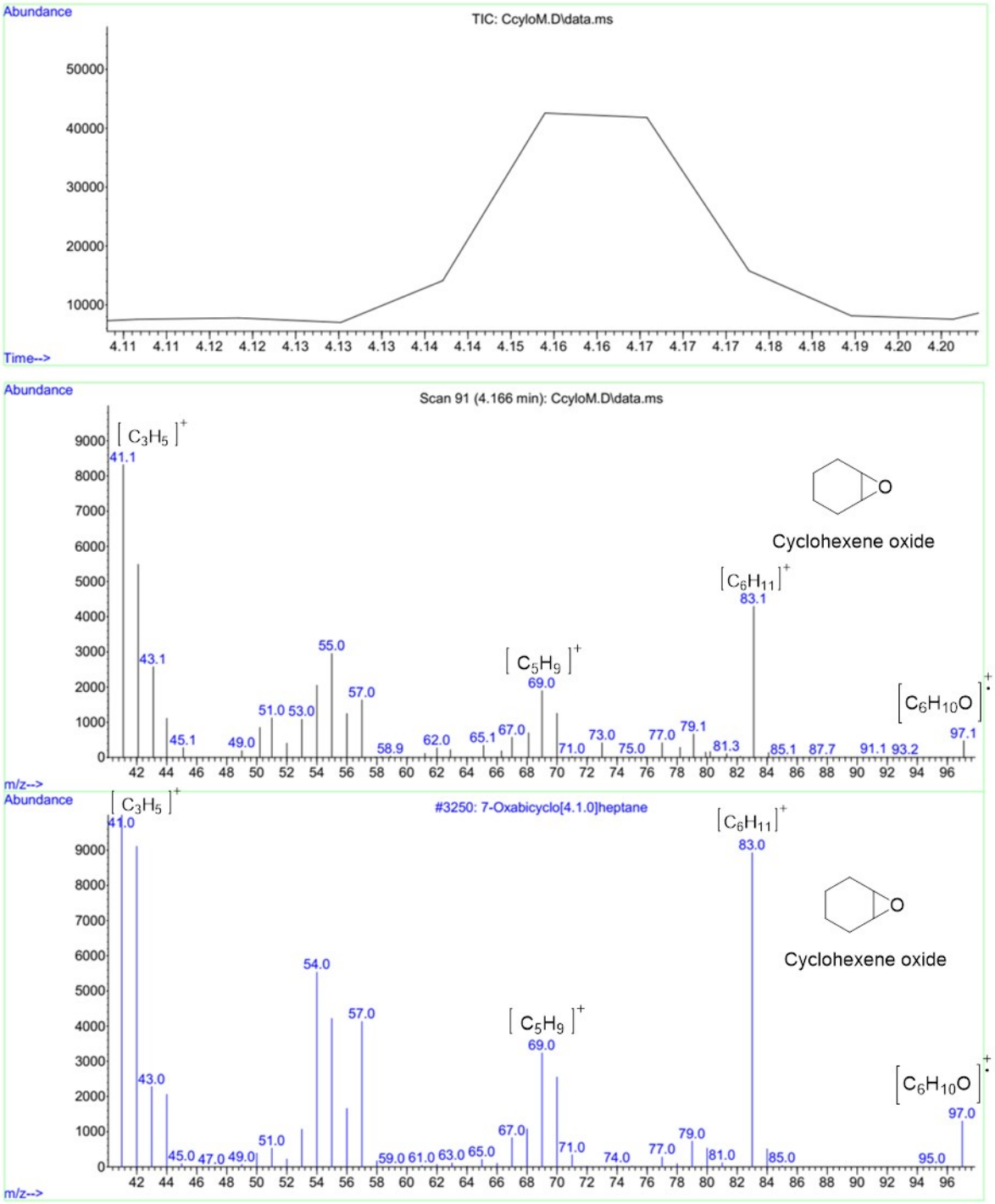

Figure S17. Mass spectrum of cyclohexene oxide.

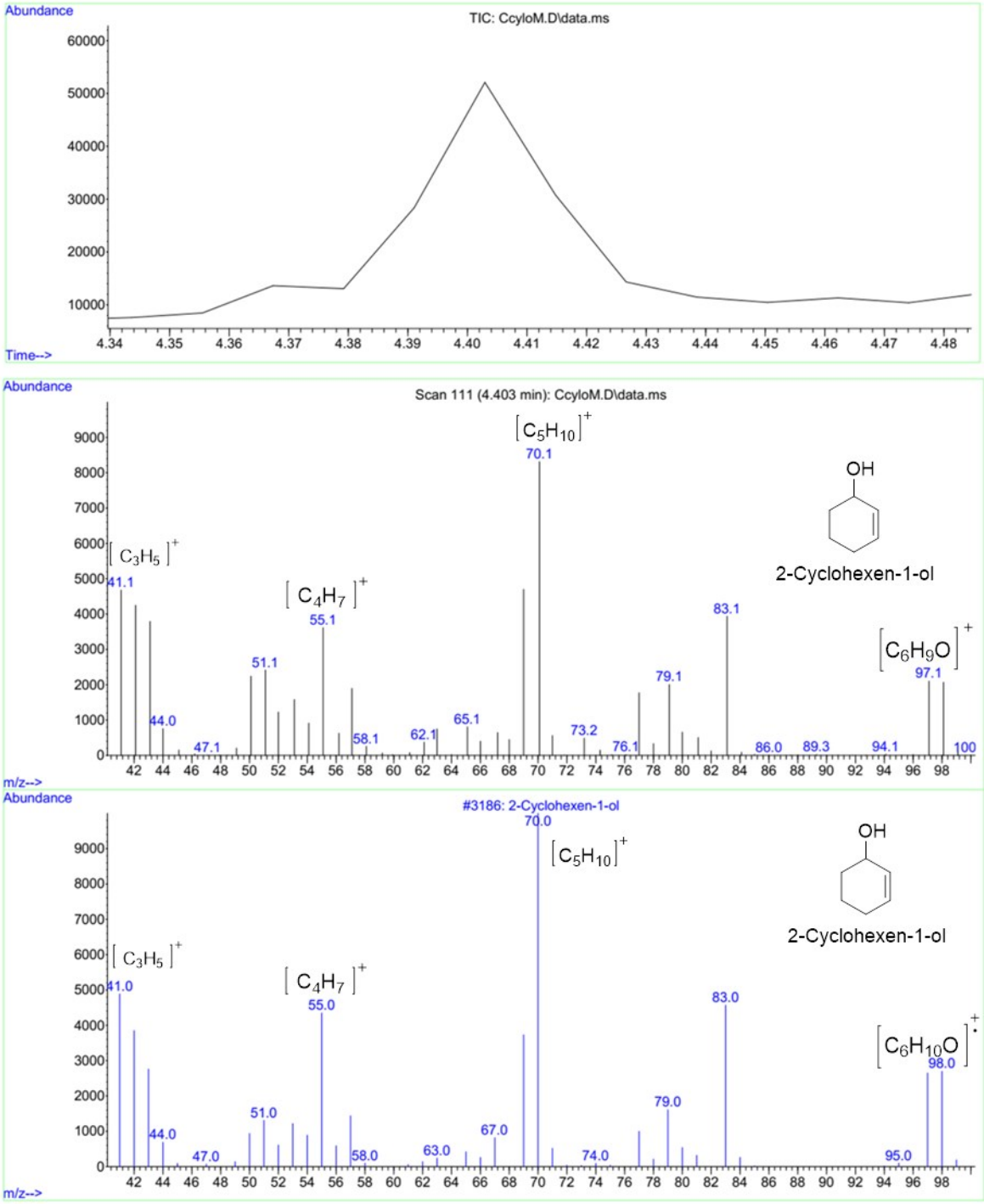

Figure S18. Mass spectrum of 2-cyclohexene-1-ol.

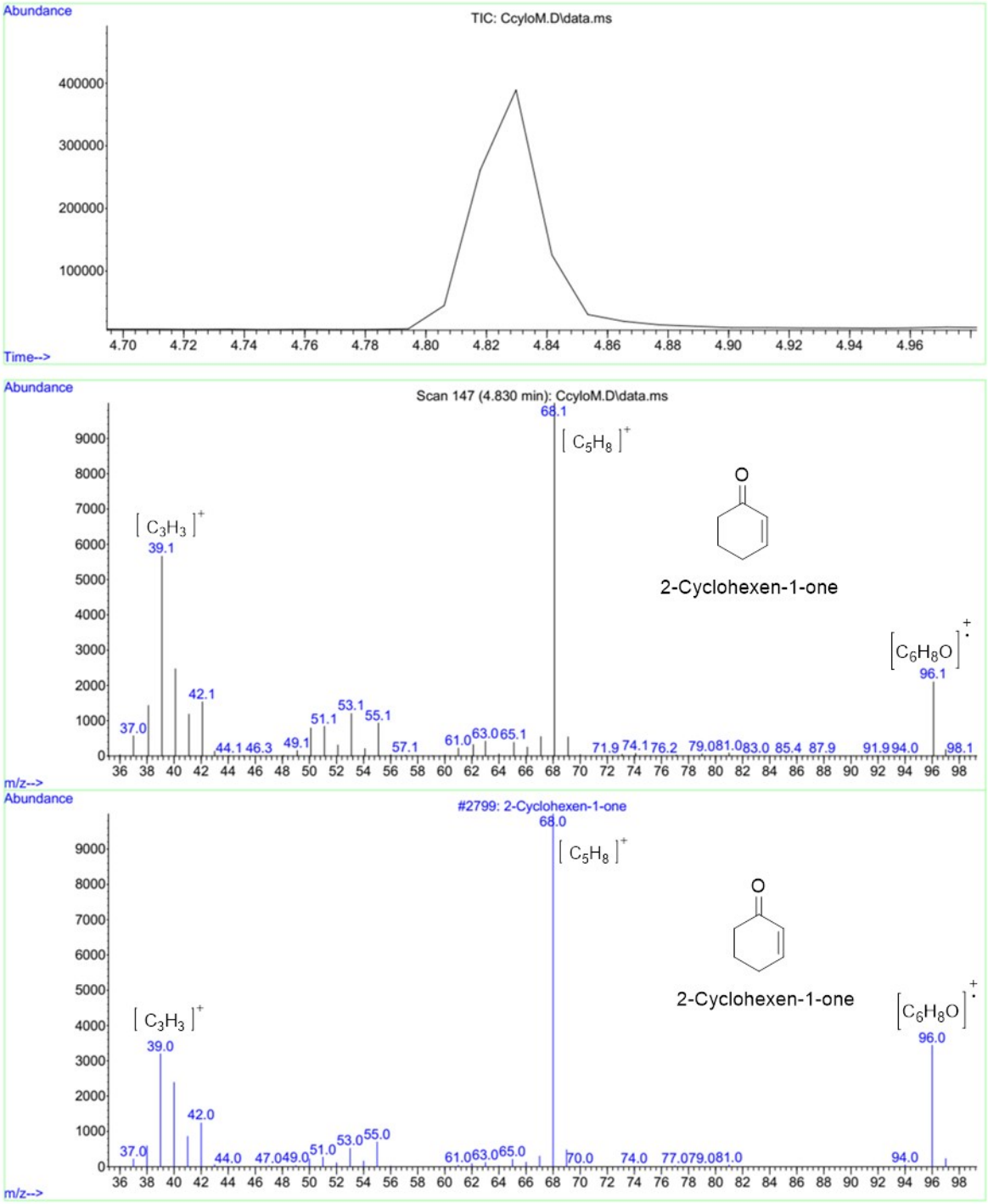

Figure S19. Mass spectrum of 2-cyclohexene-1-one.

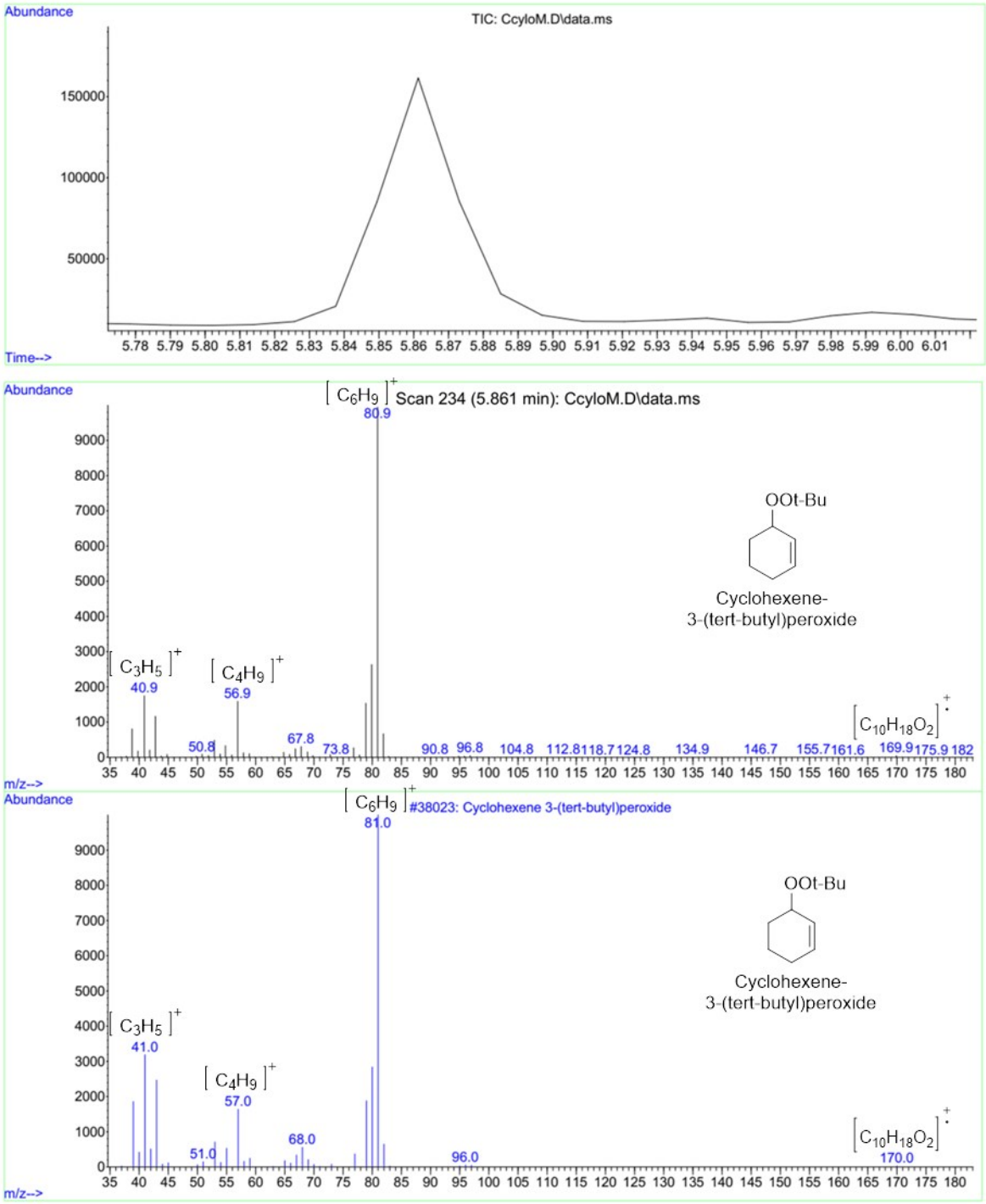

Figure S20. Mass spectrum of cyclohexene-3-(*tert*-butyl)peroxide.

Section S5: Post-catalysis Characterization of Ce-MOF-589.

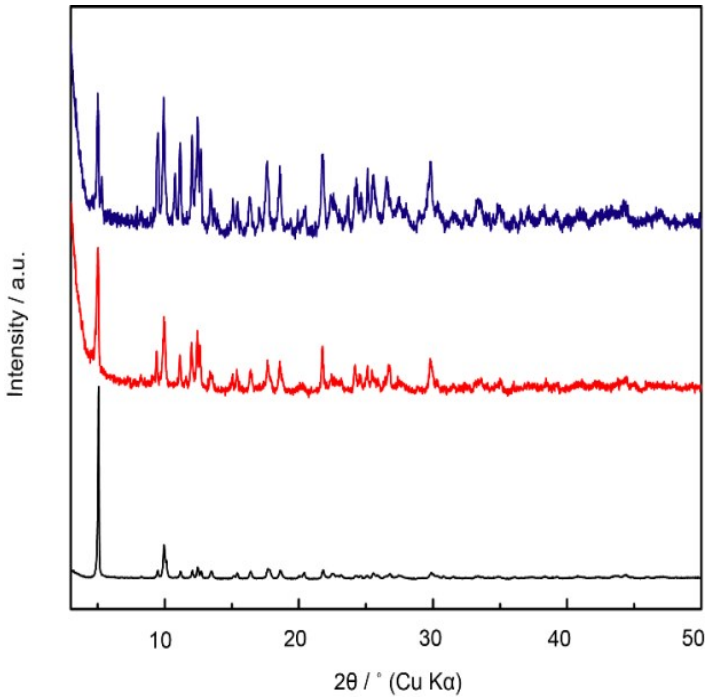

Figure S21. Comparison of the PXRD patterns of the fresh (black), after 1st cycle (red), and after 6th cycle (blue) reactions for Ce-MOF-589 catalyst.

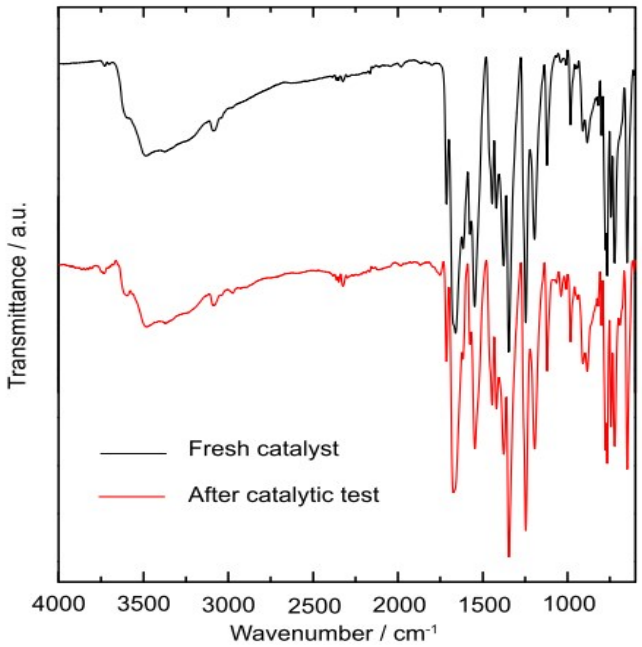

Figure S22. FT-IR of an activated Ce-MOF-589 (black) and after 6th time recycling and reusing of Ce-MOF-589 (red).

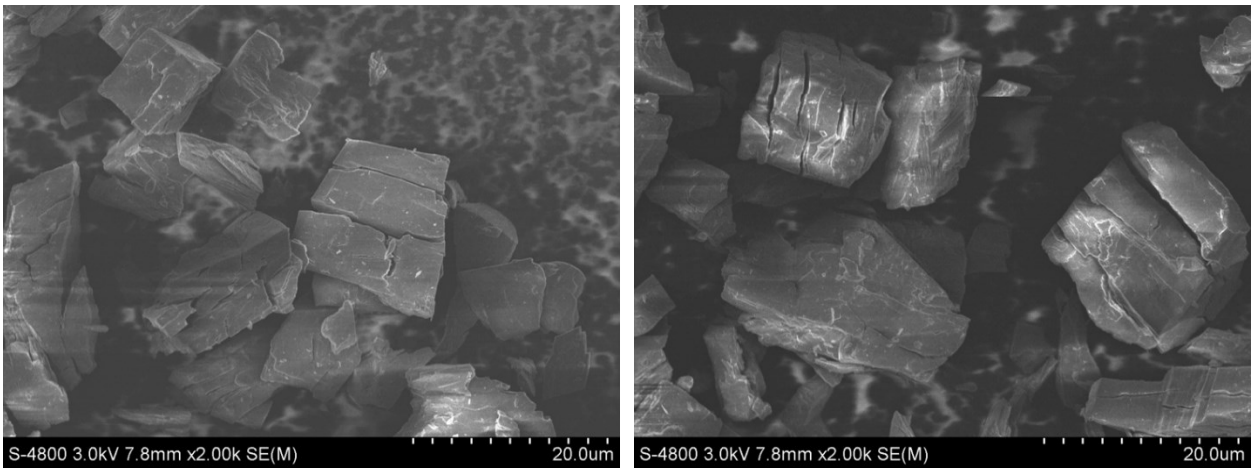

Figure S23. SEM images of the Ce-MOF-589 before (left) and after (right) catalytic reactions.

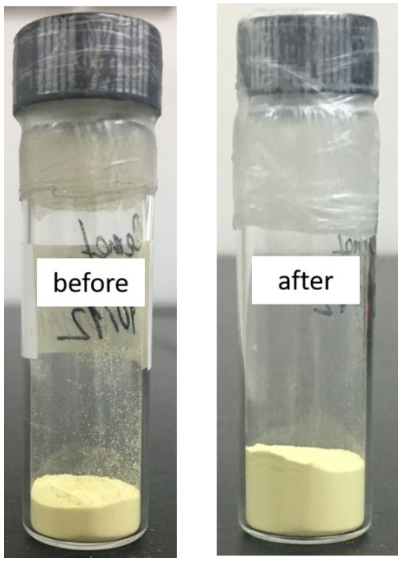

Figure S24. Color of bulk-scale of Ce-MOF-589 sample before (left) and after (right) catalytic reactions.

Section S6: References

[S1] N. L. Rosi, J. Kim, M. Eddaoudi, B. Chen, M. O'Keeffe and O. M. Yaghi, *J. Am. Chem. Soc.*, 2005, **127**, 1504-1518.